Microsc. Microanal. 22, 1374–1380, 2016
doi:10.1017/S143192761601182X

Microscopy AND Microanalysis

A Mathematical Model for Determining Carbon Coating Thickness and Its Application in Electron Probe Microanalysis

Ruo-Xi Zhang, and Shui-Yuan Yang*

State Key Laboratory of Geological Processes and Mineral Resources, China University of Geosciences, Wuhan 430074, PR China

Abstract: In electron probe microanalysis where materials are coated with a thin conductive carbon coat before analysis, the X-ray intensity detected from a specimen may be affected to various degrees by the thickness of the carbon coating. Differences in the carbon film thickness between specimens and standards may lead to errors in analytical results, particular for lower energy X-rays. In this study, we demonstrate that the location and the distance of the specimen relative to the carbon tip in the coating chamber can affect the thickness of the carbon film produced on the specimen surface during carbon coating. The closer the specimen is to the carbon tip contacting point, the thicker is the carbon film deposited. A mathematical model to calculate the carbon film thickness at different locations on the coater plate is established, based on the assumption that carbon atoms evaporate from the carbon tip equally in all directions during the coating process. In order to reduce the differences in the carbon coating thickness, we suggest moving the carbon rod to a higher position, moving the thinner samples to the center and thicker samples to the edge of the coater plate, and using a rotating circular coater plate during coating.

Key words: electron probe microanalysis, carbon coating, film thickness variation, film thickness calculation

Introduction

Electron probe microanalysis (EPMA) is one of the most commonly used analytical techniques for determining the concentration of most elements in a solid material (e.g., McGee & Keil, 2001; Zhao et al., 2015). During EPMA, samples with poor electrical conductivity (e.g., geological specimens) accumulate charge on the sample surface from the high-energy beam electron, producing the "charging" phenomenon. Here there is a decrease in the effective "landing electron beam energy", influencing the generation of secondary and backscattered electrons and most critically, characteristic X-rays. Therefore, a non-conductive sample must be coated with a thin surface layer of conductive material to avoid the charging effect and, second, to reduce sample heating (Limandri et al., 2010). Carbon coating is usually applied as carbon is conductive and provides no X-ray interference to lines being quantified (e.g., Kerrick et al., 1973; Limandri et al., 2010; Zhao et al., 2015). However, a carbon film coating on the sample surface will absorb the energies of incident electrons and of emitted X-rays, resulting in decreased X-ray intensity (Sweatman & Long, 1969; Reed, 1972; Kerrick et al., 1973; Kato, 2007; Limandri et al., 2010; Buse & Kearns, 2015). Most critically, differences between the carbon film thicknesses on specimens and on standards can lead to errors in the X-ray intensity measurement (Kerrick et al., 1973). Therefore, coating standards and specimens together has been suggested to avoid the effects of discrepancies in carbon coating thickness in quantitative analysis. However, it is impractical to always coat standards and unknown specimens together, as this requires the standards to be cleaned and recoated with each specimen batch. Methods to control and determine the thickness have been developed (Limandri et al., 2010, and references therein), but these techniques are complex, operationally difficult, and can obtain only one measurement of the film thickness.

In this study, we establish a mathematical model to calculate the thickness of carbon coating and propose a strategy for alleviating differences in the film thickness during a coating process.

Received April 4, 2016; accepted September 22, 2016
*Corresponding author. shuiyuanyang@cug.edu.cn

Materials and Methods

Carbon Coating

Carbon coating was carried out using a JEOL JEE-420 vacuum evaporator (JEOL Ltd., Tokyo, Japan) at the State Key Laboratory of Geological Processes and Mineral Resources, China University of Geosciences (CUG) at Wuhan. Two cylindrical carbon rods were used, each with a diameter of 5 mm. One of the rods was sharpened to a smaller cylindrical carbon tip (about 1 mm in diameter) with a flat end, and the other was not sharpened (Fig. 1). A 100-mm-long polished brass strip was placed on a round, flat, and stationary sample plate with a diameter of about 200 mm. One end of the brass strip was placed directly below the point where the carbon rods contacted each other (hereafter called the tip contacting point), at the center of the sample plate. The brass strips were then coated at a vertical distance from the carbon tip contacting point of 50 and 75 mm.

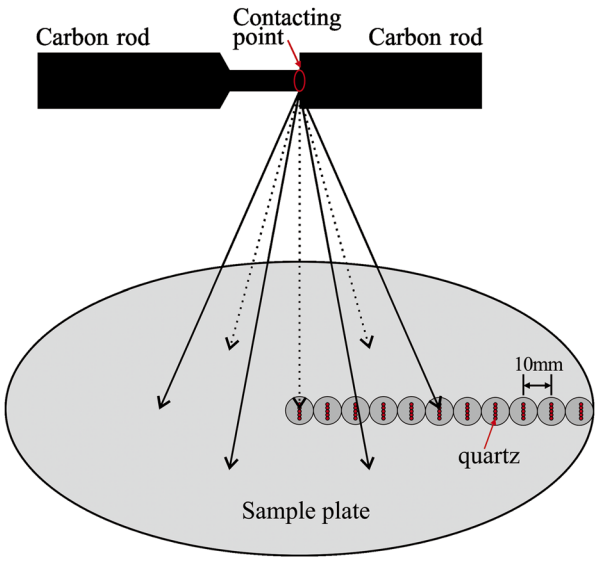

Figure 1. The relevant structure of a vacuum evaporator containing carbon rods, sample plate, and specimens.

The total mass of carbon evaporated during one coating event was determined by accurately weighing the carbon rod before coating, and after coating, using a sensitive electronic scale.

In total, 11 rows of quartz grains enclosed in epoxy resin were prepared. Each row contained five quartz grains (G1–G5) that were ground and polished until the crystals were approximately at their maximum width. These samples were arranged, with even spacing, from the center of the sample plate to the outer edge. The interval between adjacent samples was 10 mm along a straight line (Fig. 1). The first quartz sample in the center of the sample plate was placed directly below the carbon tip contacting point. A 100-mm-long polished brass strip was also placed beside the quartz grains. The brass strip was the same height as the quartz samples, with one end placed directly below the carbon tip contacting point. During coating, the carbon tip evaporated, and the estimated volume was calculated from the mass of burnt carbon and the density of the carbon film. The quartz samples and brass strips were coated with about 6.6 mm^3 of carbon with a vertical distance of 75 mm between the carbon tip contacting point and the first quartz sample at the center of the sample plate, and with about 6.2 mm^3 carbon at a vertical distance of 100 mm. A carbon rod was also mounted and polished in a similar manner to use as an analytical standard for carbon.

k-Ratio Measured by EPMA

After coating with about 6.6 mm^3 carbon at a distance of 75 mm and about 6.2 mm^3 carbon at a distance of 100 mm, the X-ray intensities of C-Kα from the surface of 55 quartz grains and the reference carbon rod were determined with an LDE2H crystal on a JEOL JXA-8100 Electron Probe Microanalyzer (JEOL Ltd., Tokyo, Japan) at CUG, Wuhan.

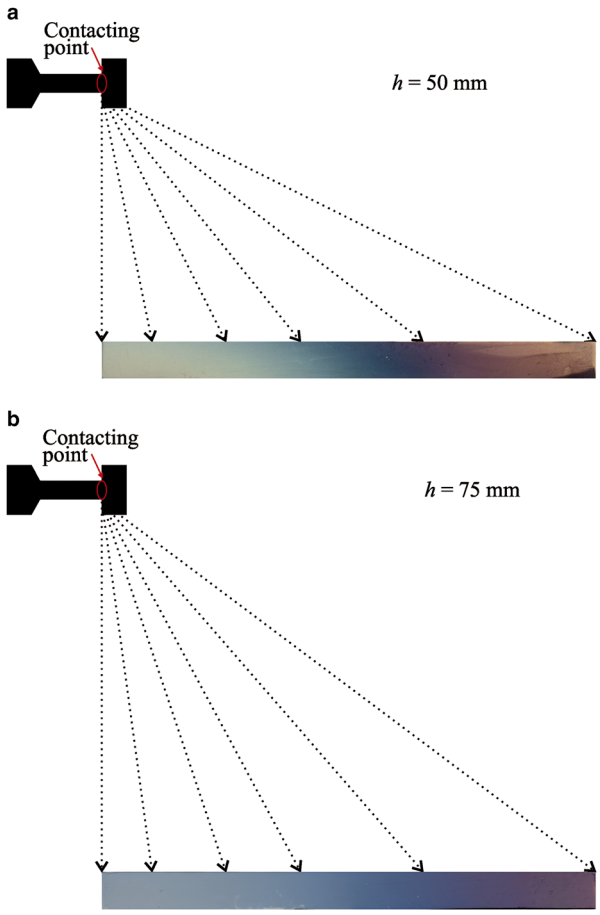

Figure 2. Variation in interference colors on a coated 100-mm-long polished brass strip using carbon tip heights of (**a**) 50 mm and (**b**) 75 mm. The far left end of the strip was directly under the carbon tip and the far right edge was at the edge of the sample plate.

In all, 11 positions on the brass strip surface, evenly spaced along the straight 100 mm line, were selected, and five points (P1–P5) of each position were selected for X-ray intensity determination with C-Kα. The *k*-ratio refers to the ratio of unknown intensity (intensities of C-Kα from quartz grains and brass strips) to standard intensity (intensities of C-Kα from carbon rod). Experimental conditions were accelerating voltages of 5 and 10 kV for quartz grains, and 15 and 20 kV for brass strips, a beam current of 20 nA, and a defocused 10 μm diameter electron beam.

Results and Discussion

Thickness Variation

The carbon atoms are assumed to evaporate in all directions from the carbon tip contacting point when the resistance heating reaches a high temperature. If a position on the surface of the specimen being coated was closer to the carbon tip contacting point, it would have more carbon deposited. Therefore, specimens placed in different positions inside the vacuum evaporator would have carbon coatings of different thicknesses.

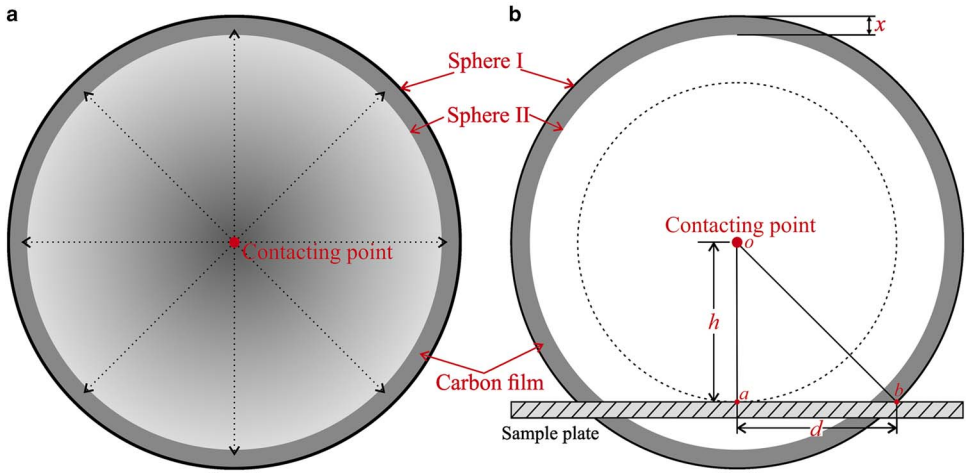

Figure 3. a: Schematic diagram of the carbon evaporation assuming a spherical geometry (plan view). **b:** Hypothetical vertical slice, showing model calculation of carbon coating thickness. *x*, carbon film thickness; *o* carbon tip contacting point; *h* height of carbon tip contacting point relative to the sample plate; *d*, distance between any point on the sample plate and the point vertically below the carbon tip contacting point.

Interference colors of carbon films deposited on the brass surface provide a useful estimate for the variation in thickness (Kerrick et al., 1973). Figure 2 shows that interference colors on the 100-mm-long polished brass strips from the same evaporation changed from silver or light blue at the far left to orange at the far right, indicating different carbon coating thicknesses, from maximum to minimum thickness.

Mathematical Model

Techniques used to measure carbon coating thickness include the Dektak profilometer (Sloan Research Industries Inc., United States), which can track over a vertical edge of the carbon film using a diamond stylus and provide a direct measurement of film thickness (Kerrick et al., 1973); sputter depth profiling (Hofmann, 1998); X-ray photoelectron spectroscopy (Alexander et al., 2002); reference-free fundamental parameter-based X-ray fluorescence analysis (Kolbe et al., 2005); and X-ray reflectometry (Thomsen-Schmidt et al., 2004). However, these techniques involve complicated and difficult data processing (e.g., Limandri et al., 2010) and acquire only one thickness measurement. The utilization of a quartz crystal oscillator monitor to measure carbon coating thickness is a convenient method, but, again, only one thickness measurement can be acquired, at the position of the monitor. Thus, these techniques are of limited use in carbon vacuum evaporation.

During carbon evaporation, the carbon atoms emit concentrically from the carbon tip contacting point in all directions (Fig. 3a). Assuming the carbon tip contacting point is at the center of sphere I, the distance between location *b* on the sample plate and the carbon tip contacting point is the inner radius of the sphere (Fig. 3b). During carbon coating, assuming that the carbon atoms are not blocked from their emitted path, the evaporated carbon atoms would evenly deposit on the internal surface of the sphere (Fig. 3a). After carbon coating, the inner radius of the

Table 1. Carbon Coating Thickness (*x*) Depending on Typical *h* and *d* Values.

	x (nm)				
d (mm)	$h = 50$ mm; $V = 1.257$ mm^3	$h = 75$ mm; $V = 2.827$ mm^3	$h = 100$ mm; $V = 5.027$ mm^3	$h = 125$ mm; $V = 7.854$ mm^3	$h = 150$ mm; $V = 11.31$ mm^3
0	40.0	40.0	40.0	40.0	40.0
10	38.5	39.3	39.6	39.7	39.8
20	34.5	37.3	38.5	39.0	39.3
30	29.4	34.5	36.7	37.8	38.5
40	24.4	31.1	34.5	36.3	37.3
50	20.0	27.7	32.0	34.5	36.0
60	16.4	24.4	29.4	32.5	34.5
70	13.5	21.4	26.8	30.5	32.8
80	11.2	18.7	24.4	28.4	31.1
90	9.4	16.4	22.1	26.3	29.4
100	8.0	14.4	20.0	24.4	27.7

Table 2. Comparison of the Measured and Calculated *k*-ratios of C from GMRFilm (Waldo, 1988).

Quartz Grains

			k-Ratio Measured at 5 kV						*k*-Ratio Measured at 10 kV				
d (mm)	*x* (nm)	*k*-Ratio Calculated at 5 kV	G1	G2	G3	G4	G5	*k*-Ratio Calculated at 10 kV	G1	G2	G3	G4	G5
$h = 75$ mm, $V = 6.6$ mm^3													
0	93.4	0.267	0.301	0.295	0.295	0.295	0.295	0.086	0.093	0.093	0.092	0.092	0.093
10	91.7	0.261	0.282	0.281	0.279	0.280	0.277	0.084	0.088	0.088	0.087	0.087	0.087
20	87.2	0.247	0.247	0.248	0.247	0.249	0.249	0.080	0.079	0.079	0.079	0.079	0.083
30	80.5	0.225	0.213	0.212	0.213	0.212	0.213	0.073	0.068	0.068	0.069	0.068	0.068
40	72.7	0.201	0.178	0.178	0.178	0.178	0.178	0.065	0.057	0.057	0.057	0.057	0.057
50	64.6	0.176	0.148	0.148	0.149	0.149	0.149	0.057	0.049	0.048	0.049	0.048	0.048
60	56.9	0.152	0.124	0.123	0.124	0.124	0.125	0.050	0.040	0.040	0.040	0.041	0.041
70	49.9	0.131	0.106	0.105	0.106	0.106	0.105	0.043	0.036	0.034	0.035	0.035	0.035
80	43.7	0.113	0.091	0.091	0.093	0.092	0.092	0.038	0.030	0.030	0.030	0.030	0.030
90	38.3	0.097	0.081	0.079	0.080	0.080	0.081	0.033	0.027	0.026	0.027	0.027	0.027
100	33.6	0.084	0.071	0.071	0.073	0.074	0.074	0.029	0.024	0.024	0.024	0.025	0.024
$h = 100$ mm, $V = 6.2$ mm^3													
0	49.3	0.129	0.149	0.146	0.146	0.148	0.148	0.043	0.046	0.045	0.045	0.046	0.047
10	48.9	0.128	0.142	0.143	0.143	0.144	0.145	0.042	0.044	0.044	0.044	0.044	0.045
20	47.4	0.124	0.137	0.136	0.137	0.138	0.138	0.041	0.043	0.043	0.043	0.043	0.043
30	45.3	0.118	0.127	0.128	0.130	0.129	0.130	0.039	0.040	0.039	0.040	0.040	0.041
40	42.5	0.110	0.118	0.119	0.119	0.120	0.120	0.037	0.037	0.038	0.037	0.038	0.037
50	39.5	0.101	0.107	0.107	0.107	0.107	0.107	0.034	0.034	0.033	0.034	0.033	0.033
60	36.3	0.092	0.095	0.095	0.096	0.096	0.097	0.031	0.030	0.030	0.031	0.031	0.031
70	33.1	0.083	0.088	0.088	0.089	0.089	0.090	0.028	0.028	0.028	0.029	0.028	0.028
80	30.1	0.075	0.082	0.083	0.083	0.084	0.086	0.025	0.026	0.026	0.027	0.027	0.027
90	27.3	0.067	0.081	0.080	0.081	0.080	0.079	0.023	0.026	0.027	0.026	0.025	0.025
100	24.7	0.060	0.074	0.073	0.073	0.073	0.073	0.021	0.024	0.024	0.023	0.023	0.023

Brass strips

			k-Ratio Measured at 15 kV						*k*-Ratio Measured at 20 kV				
d (mm)	*x* (nm)	*k*-Ratio calculated at 15 kV	P1	P2	P3	P4	P5	*k*-Ratio calculated at 20 kV	P1	P2	P3	P4	P5
$h = 75$ mm, $V = 6.6$ mm^3													
0	93.4	0.077	0.088	0.085	0.084	0.087	0.083	0.064	0.069	0.069	0.068	0.068	0.067
10	91.7	0.076	0.077	0.078	0.077	0.077	0.075	0.062	0.067	0.064	0.064	0.065	0.063
20	87.2	0.072	0.069	0.069	0.069	0.070	0.069	0.059	0.058	0.058	0.058	0.058	0.057
30	80.5	0.066	0.061	0.060	0.059	0.059	0.056	0.055	0.050	0.050	0.049	0.049	0.047
40	72.7	0.059	0.051	0.051	0.051	0.050	0.050	0.049	0.042	0.042	0.043	0.042	0.042
50	64.6	0.053	0.043	0.043	0.043	0.043	0.042	0.044	0.037	0.037	0.038	0.035	0.035
60	56.9	0.046	0.037	0.036	0.036	0.038	0.035	0.038	0.030	0.031	0.029	0.030	0.029
70	49.9	0.040	0.031	0.032	0.032	0.031	0.031	0.033	0.027	0.026	0.026	0.026	0.026
80	43.7	0.035	0.028	0.027	0.028	0.028	0.028	0.029	0.023	0.023	0.023	0.022	0.022
90	38.3	0.030	0.027	0.027	0.027	0.026	0.027	0.025	0.022	0.023	0.021	0.021	0.024
100	33.6	0.027	0.023	0.024	0.024	0.023	0.022	0.022	0.020	0.019	0.020	0.021	0.020
$h = 100$ mm, $V = 6.2$ mm^3													
0	49.3	0.039	0.043	0.044	0.043	0.043	0.043	0.033	0.035	0.035	0.037	0.035	0.036
10	48.9	0.039	0.041	0.041	0.040	0.040	0.042	0.033	0.034	0.034	0.033	0.034	0.034
20	47.4	0.038	0.038	0.039	0.039	0.039	0.039	0.032	0.032	0.032	0.032	0.032	0.034
30	45.3	0.036	0.036	0.036	0.037	0.036	0.037	0.030	0.030	0.030	0.030	0.031	0.031
40	42.5	0.034	0.034	0.033	0.033	0.035	0.033	0.028	0.028	0.028	0.028	0.028	0.029
50	39.5	0.031	0.031	0.031	0.031	0.032	0.031	0.026	0.026	0.025	0.026	0.025	0.026
60	36.3	0.029	0.028	0.029	0.029	0.030	0.028	0.024	0.023	0.024	0.023	0.023	0.023
70	33.1	0.026	0.026	0.027	0.027	0.029	0.028	0.022	0.021	0.022	0.021	0.022	0.022
80	30.1	0.024	0.024	0.024	0.024	0.024	0.025	0.020	0.020	0.020	0.020	0.020	0.020
90	27.3	0.021	0.023	0.023	0.023	0.024	0.023	0.018	0.019	0.019	0.019	0.019	0.020
100	24.7	0.019	0.022	0.025	0.025	0.022	0.023	0.016	0.019	0.019	0.019	0.018	0.019

sphere would become smaller due to the deposition of carbon, with this change being approximately equal to the carbon coating thickness (x) at location b on the sample plate. A mathematical model to calculate the carbon film thickness at location b can be established, assuming that the inner sphere after carbon coating is sphere II, the distance between the carbon tip contacting point o and location a on the sample plate is h, and the distance between locations a and b on the sample plate is d, and that the volume of the carbon film V_{carbon} was equal to the difference in the volume between sphere I and sphere II:

$$\frac{4}{3}\pi\left(\sqrt{h^2+d^2}\right)^3-\frac{4}{3}\pi\left(\sqrt{h^2+d^2}-x\right)^3=V_{carbon}=\frac{m_o-m_f}{\rho}, \quad (1)$$

where m_o and m_f are the mass of the carbon rod before and after coating, respectively; ρ is the carbon film density (1.9 g/cm^3; Buse & Kearns, 2015). As parameters h, d, m_o,

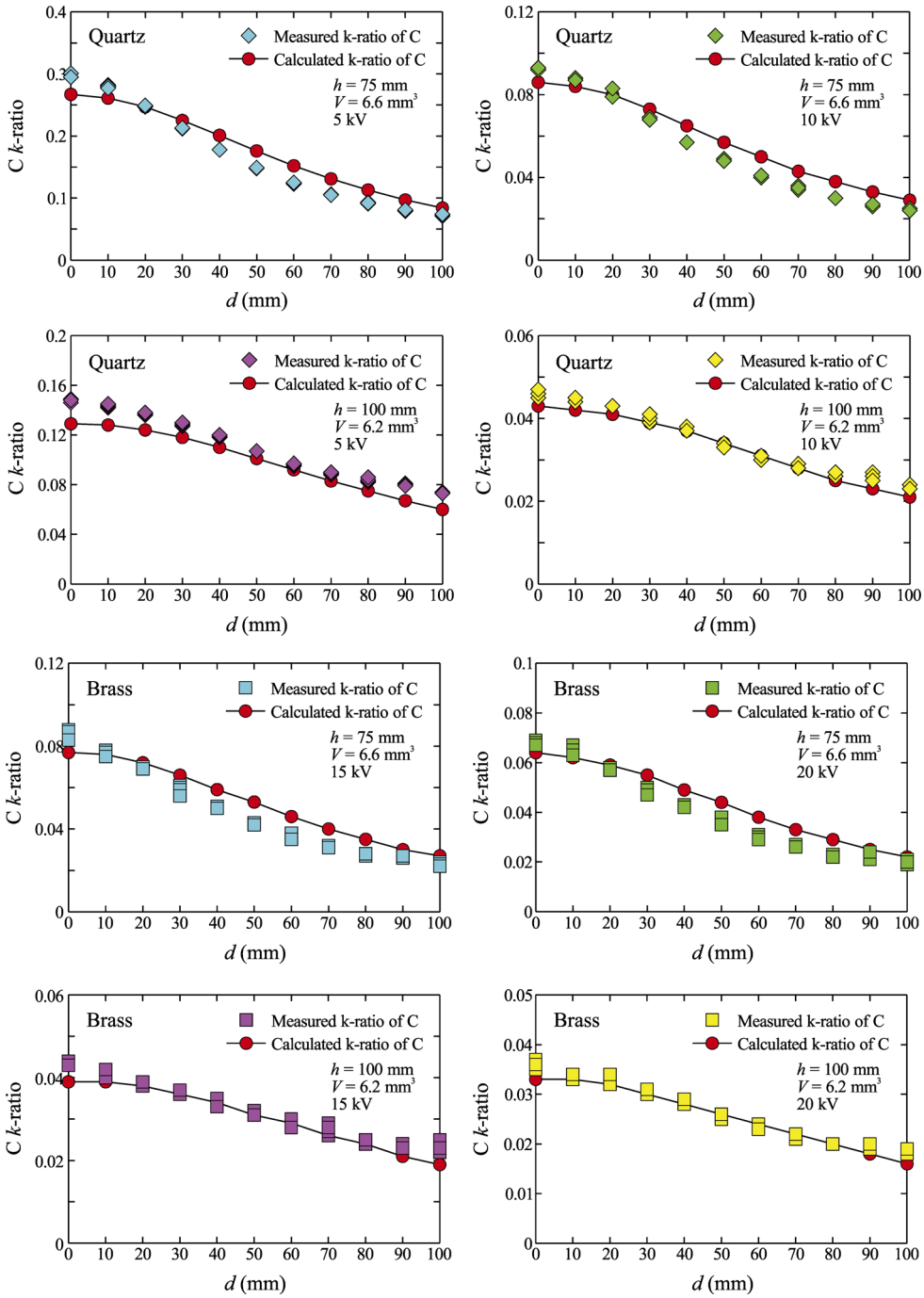

Figure 4. Graphs comparing the measured and calculated k-ratios of C. The measured k-ratio of C was calculated from the measured C-Kα intensity data on the quartz grains and brass strips. The calculated k-ratio of C in quartz grains and brass strips was obtained by matching the film thickness data from equation (1) to the theoretical output from the GMRFilm program (Waldo, 1988).

and m_f can be measured, the carbon film thickness (x) can be calculated using equation (1). Table 1 shows that carbon film thickness (x) depending on typical h and d, with the volume of the carbon film (V_{carbon}) adjusted to ensure that the carbon film thickness (x) of the origin on the sample plate was 40 nm at different distances from the carbon tip contacting point.

A self-consistency test was then performed with the GMRFilm thin film program (Waldo, 1988), using the calculated film thickness data from equation (1) to generate theoretical k-ratios for C on the quartz grains and brass strips. The GMRFilm program generates, using as input a film of a given composition, density (here 1.9 g/cm^3) and film thickness atop some substrate, a theoretical k-ratio, using a phi-rho-z X-ray generation model. To verify the accuracy of the k-ratio calculated from equation (1), the k-ratio of carbon was also measured directly using the electron probe microanalyzer.

The results are given in Table 2. The measured and calculated k-ratios of C were in excellent agreement (Fig. 4), indicating that the mathematical model for calculating the carbon film thickness was reliable.

Model Application

Using point a on the sample plate, which was directly below the carbon tip contacting point, as the origin, the distance between any other point on the sample plate and the origin, d, could be measured. Therefore, for a given carbon tip contacting point height, h, and a given volume of the carbon film, V_{carbon}, the carbon film thickness can be calculated using equation (1). V_{carbon} was adjusted to ensure that the carbon film thickness (x) at point a was 40 nm at different h (data in Table 1). Figure 5 plots the lateral distribution of the carbon film thickness on the sample plate at different carbon tip contacting point heights. As is to be expected, the carbon film became thinner moving from the origin to the edge of the sample plate. The variations in the carbon film thickness were also affected by the height of the carbon tip contacting point relative to the sample plate. When the carbon tip contacting point height was reduced from 150 to 50 mm, variation in the carbon film thickness became more significant. Therefore, at a higher carbon rod position, the coated carbon film becomes more uniform with lateral distance from the origin. This was also evidenced by the color of brass strips carbon coated using different carbon tip contacting point heights (Fig. 2).

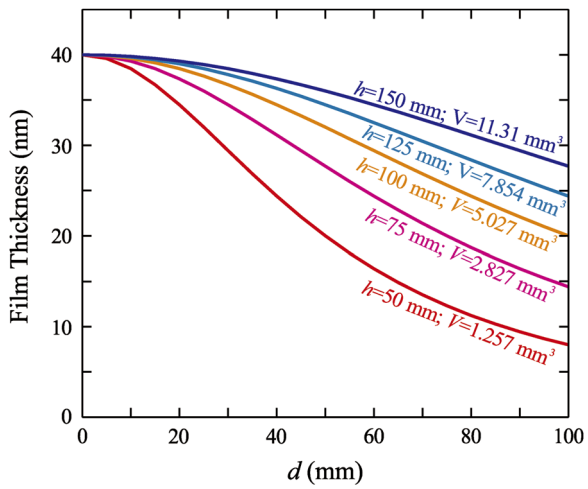

Figure 5. Schematic diagram showing the distribution of the carbon film thickness on the sample plate during the same evaporation using different carbon tip contacting point heights. The point on the sample plate vertically below the carbon tip contacting point is set as the origin; the distance between any point on the sample plate and the origin is the X axis, and the carbon film thickness of any point on the sample plate is the Y axis. The volume of carbon film (V_{carbon}) was adjusted to ensure that the carbon film thickness (x) on the origin was 40 nm at each carbon tip contacting point height.

The total percentage loss of X-ray intensity in the carbon film derived by combining the energy loss of beam electrons and emitted X-rays absorbed by the carbon film, is defined by the following formula (Reed, 1975):

$$\Delta I = 100 + \left(\frac{8.3\times 10^4 \rho \Delta z}{V_o^2 - V_c^2} - 100\right)\exp\left(-\left(\frac{\mu}{\rho}\right)\rho \Delta z \csc\theta\right), \quad (2)$$

where ΔI is the percentage X-ray intensity loss, ρ is the film density (mg/cc), z is the film thickness (cm), V_o is the accelerating voltage (kV), V_c is the critical excitation potential (kV), μ/ρ is the mass absorption coefficient of carbon for the radiation concerned, and θ is the take-off angle.

The total percentage loss in X-ray intensity would be the same if both unknown specimen and standards had the same carbon film thickness. Having the same carbon coating thickness on both specimens and standards is very important for EPMA. One approach to achieve this is to coat standards and specimens together. An alternative method is to try to consistently match the color of carbon coating produced on a piece of polished brass and/or on a white porcelain plate with an oil drop (e.g., Sweatman & Long, 1969; Kerrick et al., 1973; Buse & Kearns, 2015).

However, our study demonstrated that specimens at different distances from the carbon tip contacting point produced different carbon coating thicknesses in a single coating procedure, which could lead to errors. To minimize the effect of carbon coating thickness on EPMA, we propose the following precautions: (i) move the carbon tip contacting point to a higher position (further from the sample), as this causes the variation in the carbon film thickness to become smaller; (ii) place the thicker specimens away from the origin vertically below the carbon tip contacting point on the sample plate, and place the thinner specimens close to the origin; and (iii) use a rotating circular sample holder to hold specimens, so that all the specimens with the same thickness are approximately the same distance from the carbon tip contacting point. A rotating sample plate may also be supplied with a vacuum evaporator. However, this method may

not always produce a uniform coating when the samples are arranged from the center of the sample plate to the outer edge (Fig. 1). If samples are placed on the outer edge of the sample plate, or in a circular sample holder, then each sample should be approximately the same distance from the carbon tip contacting point, allowing an approximately uniform coating to be obtained. In this case, a rotating circular sample holder combined with a quartz crystal oscillator monitor may permit an approximately uniform coating and thickness of the carbon film.

Acknowledgments

The authors wish to thank Jian-Xiong Zhou for his help and advice during the course of this work, and Tao Luo for his help with the weighing of carbon rods. This work was financially supported by the National Natural Science Foundation of China (No. 41403022) and the Fundamental Research Funds for the Central Universities, China University of Geosciences (Wuhan) (No. CUGL150401). The authors are grateful to John Fournelle and two anonymous reviewers for providing valuable comments and suggestions, which helped to improve this manuscript significantly. Special thanks to John Fournelle for correcting the grammar and syntax of the manuscript. John Mansfield is thanked for his editorial work.

References

Alexander, M.R., Thompson, G.E., Zhou, X., Beamson, G. & Fairley, N. (2002). Quantification of oxide film thickness at the surface of aluminium using XPS. *Surf Interface Anal* **34**, 485–489.

Buse, B. & Kearns, S. (2015). Importance of carbon contamination in high-resolution (FEG) EPMA of silicate minerals. *Microsc Microanal* **21**, 594–605.

Hofmann, S. (1998). Sputter depth profile analysis of interfaces. *Rep Prog Phys* **61**, 827–888.

Kato, T. (2007). Monte Carlo study of quantitative electron probe microanalysis of monazite with a coating film: Comparison of 25 nm carbon and 10 nm gold at E_0 = 15 and 25 keV. *Geostand Geoanal Res* **31**, 89–94.

Kerrick, D.M., Eminhizer, L.B. & Villaume, J.F. (1973). The role of carbon film thickness in electron microprobe analysis. *Am Miner* **58**, 920–925.

Kolbe, M., Beckhoff, B., Krumrey, M. & ULM, G. (2005). Thickness determination for Cu and Ni nanolayers: Comparison of completely reference-free fundamental parameter-based X-ray fluorescence analysis and X-ray reflectometry. *Spectrochim Acta Part B At Spectrosc* **60**, 505–510.

Limandri, S.P., Carreras, A.C. & Trincavelli, J.C. (2010). Effects of the carbon coating and the surface oxide layer in electron probe microanalysis. *Microsc Microanal* **16**, 583–593.

McGee, J.J. & Keil, K. (2001). Application of electron probe microanalysis to the study of geological and planetary materials. *Microsc Microanal* **7**, 200–210.

Reed, S.J.B. (1972). Electron microprobe analysis at low operating voltage: Discussion. *Am Miner* **57**, 1550–1551.

Reed, S.J.B. (1975). *Electron Microprobe Analysis*. Cambridge: Cambridge University Press.

Sweatman, T.R. & Long, J.V.P. (1969). Quantitative electron-probe microanalysis of rock-forming minerals. *J Petrol* **10**, 332–379.

Thomsen-Schmidt, P., Hasche, K., Ulm, G., Herrmann, K., Krumrey, M., Ade, G., Stümpel, J., Busch, I., Schädlich, S., Schindler, A., Frank, W., Hirsch, D., Proco, P.M. & Beck, U. (2004). Realisation and metrological characterisation of thickness standards below 100 nm. *Appl Phys A* **78**, 645–649.

Waldo, R.A. (1988). An iteration procedure to calculate film compositions and thickness in electron probe microanalysis. In *Microbeam Analysis*, Newbury, D.E. (Ed.), pp. 310–314. San Francisco: San Francisco Press.

Zhao, D., Zhang, Y. & Essene, E.J. (2015). Electron probe microanalysis and microscopy: Principles and applications in characterization of mineral inclusions in chromite from diamond deposit. *Ore Geol Rev* **65**, 733–748.